Methods 244 (2025) 55–64

Contents lists available at ScienceDirect

Methods

journal homepage: www.elsevier.com/locate/ymeth

Capturing G protein-coupled receptors into native lipid-bilayer nanodiscs using new diisobutylene/maleic acid (DIBMA) copolymers☆

Ci Chu [a], Carolyn Vargas [b,c,d], Maria Carolina Barbosa [e], Simon Sommerhage [f], Gerald N. Rechberger [g], David Pahovnik [h], Ema Žagar [h], Gunnar F. Schröder [f,i], Sandro Keller [b,c,d,*], Manuel Etzkorn [a,f,**]

[a] Heinrich Heine University Düsseldorf, Faculty of Mathematics and Natural Sciences, Institute of Physical Biology, Universitätsstr. 1, 40225 Düsseldorf, Germany
[b] Biophysics, Institute of Molecular Biosciences (IMB), NAWI Graz, University of Graz, Humboldtstr. 50/III, 8010 Graz, Austria
[c] BioTechMed-Graz, Graz, Austria
[d] Field of Excellence BioHealth, University of Graz, Austria
[e] Molecular Biophysics, Technische Universität Kaiserslautern (TUK), Erwin-Schrödinger-Str. 13, 67663 Kaiserslautern, Germany
[f] Institute of Biological Information Processing (IBI-7: Structural Biochemistry), Forschungszentrum Jülich, Jülich, Germany
[g] Institute of Molecular Biosciences (IMB), NAWI Graz, University of Graz, Humboldtstr. 50/II, 8010 Graz, Austria
[h] National Institute of Chemistry, Department of Polymer Chemistry and Technology, Hajdrihova 19, Ljubljana, Slovenia
[i] Heinrich Heine University Düsseldorf, Physics Department, Universitätsstr. 1, 40225 Düsseldorf, Germany

ARTICLE INFO

Keywords:
Adrenocorticotropic hormone (ACTH)
Dynamic light scattering (DLS)
Melanocortin receptor
Membrane-protein extraction
Microfluidic diffusional sizing (MDS)
Transmission electron microscopy (TEM)

ABSTRACT

Many membrane proteins, including G protein-coupled receptors (GPCRs), are susceptible to denaturation when extracted from their native membrane by detergents. Therefore, alternative methods have been developed, including amphiphilic copolymers that enable the direct extraction of functional membrane proteins along with their surrounding lipids. Among these amphiphilic copolymers, styrene/maleic acid (SMA) and diisobutylene/maleic acid (DIBMA) polymers have been extensively studied. Despite their many benefits, SMA and DIBMA polymers also have considerable drawbacks limiting their applications. Herein, we describe a series of new amphiphilic copolymers derived from DIBMA via partial amidation of the carboxylate pendant groups with various biocompatible amines. We characterize the new polymer's nanodisc-forming properties and ability to extract the melanocortin 4 receptor (MC_4R), a prototypical class A GPCR. While each new DIBMA variant displays features that may be favorable for selected applications, we identified a PEGylated DIBMA variant called $mPEG_4$-DIBMA as particularly promising. In the tested system $mPEG_4$-DIBMA abolishes unspecific interactions and outperforms other polymers by achieving higher extraction efficiencies of MC_4R from Sf9 insect cell membranes. The new nanodisc-forming polymer combines two key advantages that are crucial for investigating GPCRs in a well-defined but still native lipid-bilayer environment, thus paving the way for manifold future applications.

1. Introduction

G protein-coupled receptors (GPCRs), the largest superfamily of cell-surface proteins, share a conserved architecture of seven transmembrane helical domains (TMDs) and have been implicated in a plethora of diseases such as cancer, obesity, and Alzheimer's disease [1–3]. The isolation of GPCRs from cellular membranes for subsequent *in vitro* studies is traditionally carried out with the aid of detergents, which displace native lipids and form micelles as a membrane-mimetic environment to solubilize GPCRs. Lipid-bilayer nanodiscs formed by membrane scaffold proteins (MSPs) have also been widely used in studies of GPCRs [4], such as neurotensin receptor 1 (NTSR1) [5], and rhodopsin [6]. However, the stability of GPCRs often decreases upon solubilization by detergents, which is the first step for preparing MSP

☆ This article is part of a special issue entitled: 'Modern membrane biophysics - Barrera' published in Methods.

* Corresponding author at: Biophysics, Institute of Molecular Biosciences (IMB), NAWI Graz, University of Graz, Humboldtstr. 50/III, 8010 Graz, Austria.
** Corresponding author at: Heinrich Heine University Düsseldorf, Faculty of Mathematics and Natural Sciences, Institute of Physical Biology, Universitätsstr. 1, 40225 Düsseldorf, Germany.
E-mail addresses: sandro.keller@uni-graz.at (S. Keller), manuel.etzkorn@hhu.de (M. Etzkorn).

https://doi.org/10.1016/j.ymeth.2025.08.013
Received 29 July 2025; Received in revised form 25 August 2025; Accepted 28 August 2025
Available online 4 September 2025

nanodiscs [4]. In addition, GPCR activities are regulated by various physical properties of the surrounding phospholipid bilayer such as lipid order, lateral pressure, bilayer thickness, hydrophobic mismatch, membrane fluidity, curvature, and lipid composition, which are altered in detergent micelles and difficult to mimic in synthetic lipid mixtures [7–10]. The lipid environment also plays critical roles in GPCR–ligand interactions, receptor coupling, and the recruitment of GPCR kinases (GRKs) and arrestins [11–14]. Therefore, the study of GPCRs in more native-like environments is highly desirable.

In addition to model membrane systems [15], significant progress has been made in developing and exploiting lipid-bilayer nanodiscs encapsulated by amphiphilic copolymers that directly extract membrane proteins together with their surrounding lipids from cellular membranes [16]. These native nanodiscs often preserve the structural and functional integrity of extracted proteins. One of the most commonly used copolymers is styrene/maleic acid polymer SMA(2:1), a negatively charged random polymer employed to purify membrane proteins from different cell types [17–22]. However, the efficiency of membrane-protein extraction by SMA(2:1) and the characterization of SMA-encapsulated proteins are restricted by a rather narrow buffer range, excluding lower pH values and even low concentrations (2 mM) of divalent cations such as Mg^{2+} and Ca^{2+} [23,24]. New strategies could overcome some of the limitations in terms of buffer compatibility [25,26], but the quantification of encapsulated proteins and several other biophysical experiments are hampered by SMA's strong absorption in the UV range, which is due to its aromatic styrene moieties. Diisobutylene/maleic acid (DIBMA) is an alternating copolymer that does not contain any aromatic groups but retains the ability to solubilize membrane proteins and lipids [27]. Thus, one of the significant advantages of DIBMA is its lower absorption in the UV range. Moreover, DIBMA exhibits only a gentle impact on the lipid acyl chain order and a high resistance against divalent cations (>20 mM) [28]. DIBMA has been successfully used to extract a broad range of membrane proteins from different host cells, including rhomboid proteases [29], the membrane tether protein ZipA [30], the ATP Binding Cassette (ABC) transporter BmrA [30], the GPCRs adenosine A_{2A} receptor ($A_{2A}R$) [30] and calcitonin gene-related peptide receptor (CGRP) [30], as well as the mechanosensitive channel of small conductance (MscS)-like channel YnaI [31]. Nonetheless, the high charge densities carried by both SMA and DIBMA, which are due to their carboxylic acid pendant groups, can interfere with binding measurements using charged ligands through unspecific Coulombic interactions.

In this work, we describe a series of new amphiphilic copolymers, including Dab-DIBMA, Arg-DIBMA, Meg-DIBMA, and $mPEG_4$-DIBMA obtained from DIBMA via partial amidation with various biocompatible amines. The formation of nanodiscs by exposing large unilamellar vesicles (LUVs) to polymers, the morphology of the resulting nanodiscs, and the thermotropic phase behavior of the encapsulated lipid bilayers were examined with the aid of dynamic light scattering (DLS), transmission electron microscopy (TEM), and differential scanning calorimetry (DSC), respectively. Additionally, microfluidic diffusional sizing (MDS) was used to gauge potential unspecific interactions between peptide ligands and polymers. The efficacies of the new polymers in extracting a prototypical GPCR were assessed by using the human melanocortin 4 receptor (MC_4R) expressed in insect cells. The results of our study demonstrate that all of the polymers examined are able to form lipid-bilayer nanodiscs with narrow size distributions. Furthermore, all polymers can extract MC_4R into native nanodiscs, providing new tools for the structural and functional characterization of GPCRs. Notably, we found that $mPEG_4$-DIBMA does not display any unspecific interactions with a cationic peptide ligand and exhibits only low UV absorption. In addition, $mPEG_4$-DIBMA is highly water-soluble, readily solubilizes phospholipid vesicles, and efficiently extracts MC_4R from insect membranes. Taken together, our study demonstrates that $mPEG_4$-DIBMA is an outstanding amphiphilic copolymer for investigating integral membrane proteins in their native lipid environment.

2. Materials and methods

2.1. Materials

The zwitterionic, saturated phospholipid 1,2-dimyristoyl-*sn*-glycero-3-phosphocholine (DMPC) was obtained from Avanti Polar Lipids (Alabaster, USA). DIBMA monomethyl ester was a kind gift from Glycon Biochemicals (Luckenwalde, Germany). Styrene/maleic acid (SMA (2:1)) copolymer was purchased from Orbiscope (Geleen, The Netherlands). *n*-Dodecyl-β-D-maltopyranoside (DDM) was from Glycon Biochemicals (Luckenwalde, Germany). L-Arginine was purchased from Carl Roth (Karlsruhe, Germany), meglumine from Fisher Scientific (Schwerte, Austria), and L-2,4-diaminobutyric acid dihydrochloride from Bachem (Bubendorf, Switzerland). $MgCl_2$, $CaCl_2$, cholesteryl hemisuccinate (CHS), tris(hydroxymethyl)aminomethane hydrochloride (Tris-HCl), 2-(4-(2-hydroxyethyl)-1-piperazinyl)-ethanesulfonic acid (HEPES), and other chemicals were purchased from Sigma–Aldrich (Darmstadt, Germany). 2,5,8,11-Tetraoxatridecan-13-amine ($mPEG_4$-amine), used for preparing $mPEG_4$-DIBMA, was synthesized as described in detail in Section 2.2.

2.2. Syntheses

All starting materials purchased from TCI (Eschborn, Germany), Fisher Scientific (Schwerte, Austria), Th. Geyer (Renningen, Germany), and Sigma–Aldrich (Darmstadt, Germany) were used as received. All four DIBMA derivatives—Arg-DIBMA, Dab-DIBMA, Meg-DIBMA, and $mPEG_4$-DIBMA—were synthesized in the same manner, following the protocol previously published for Glyco-DIBMA [32,33]. Specifically, DIBMA monomethyl ester (2 g, 8.3 mmol), which is fully esterified at one of the two carboxylate groups per repeat unit, was dissolved in 80 mL MeOH, and the appropriate amine (8.3 mmol) dissolved in 25 wt% sodium methoxide solution (4 mL diluted in 20 mL MeOH) was added under stirring at room temperature. The reaction mixture was refluxed overnight, and MeOH was removed by rotary evaporation. Amines used were L-arginine (Arg), L-2,4-diaminobutyric acid (Dab) dihydrochloride, meglumine (Meg), and tetraethyleneglycol monomethyl ether amine ($mPEG_4$-amine) for Arg-DIBMA, Dab-DIBMA, Meg-DIBMA, and $mPEG_4$-DIBMA, respectively. ^{1}H NMR and attenuated total reflection infrared (ATR-IR) spectra were recorded to verify the DIBMA amide products (Fig. S1).

The synthesis of $mPEG_4$-amine based on a previously reported procedure [34] is described below:

2,5,8,11-Tetraoxatridecan-13-yl 4-methylbenzenesulfonate (**1**)

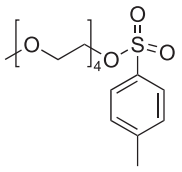

A solution of tetraethylene glycol monomethyl ether (10.0 g, 48 mmol, 1 eq.) in DCM (50 mL) was added dropwise over 30 min to a solution of *p*-toluenesulfonyl chloride (9.16 g, 48 mmol, 1 eq.) suspended in DCM (50 mL) while stirring at room temperature. Triethylamine (13.4 mL, 0.096 mmol, 2 eq.) was then added dropwise over 10 min and the reaction mixture was stirred at room temperature for 22 h. The solvent was evaporated under reduced pressure and the residue was diluted in DCM (70 mL) and washed with NaOH (1 M, 3 × 70 mL), followed by water (3 × 70 mL). The organic phase was dried over $MgSO_4$, filtered, and concentrated under reduced pressure. The resulting oil was purified by gravity column chromatography using ethyl acetate as eluent. The product was obtained as a yellowish oil in 73 % yield. The identity of the resulting product was confirmed by high-resolution mass spectrometry (HR-MS) (Fig. S2), ^{1}H NMR and ^{13}C NMR spectroscopy,

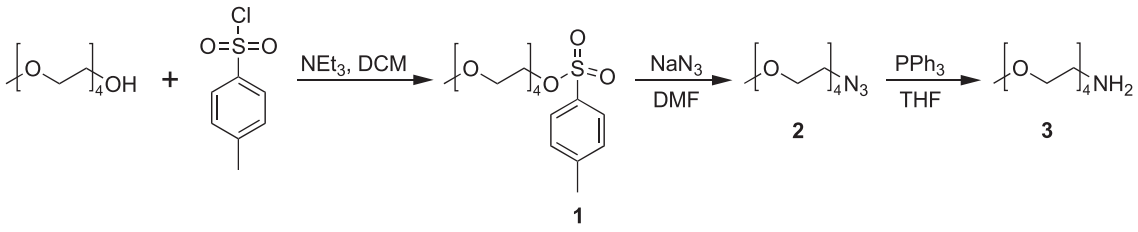

and ATR-IR spectroscopy: ^{1}H NMR [34] (300 MHz, $CDCl_3$, 25 °C): δ (ppm) = 2.39 (s, 3H, Ar–C*H*$_3$), 3.32 (s, 3H, –OC*H*$_3$), 3.45–3.66 (m, 14H, 3(–O–C*H*$_2$C*H*$_2$–O–), –OC*H*$_2$–), 4.10 (t, 2H, Ts–CH$_2$–, $^{3}J_{H-H}$ = 4.89 Hz), 7.29 (d, 2H, Ar–H, $^{3}J_{H-H}$ = 8.01 Hz), 7.74 (d, 2H, Ar–H, $^{3}J_{H-H}$ = 8.32 Hz); ^{13}C NMR [34] (75 MHz, $CDCl_3$, 25 °C): δ (ppm) = 144.9, 133.1, 129.9, 128.1, 72.0, 70.8, 70.7, 70.6, 70.6, 70.6, 69.4, 68.8, 59.1, 21.7; ATR-IR [35,36] (cm^{-1}): 2874 (C–H str, aliphatic), 1452 (C=C str, aromatic), 1353 (S=O str, asym), 1189 (S=O str, sym), 1175 (C–C str, aliphatic), 1096 (C–O–C str).

13-Azido-2,5,8,11-tetraoxatridecane (**2**)

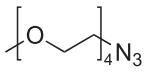

To a suspension of sodium azide (1.54 g, 23.4 mmol, 1.5 eq.) in DMF (40 mL), a solution of **1** (5.66 g, 15.6 mmol, 1.0 eq.) in DMF (25 mL) was added dropwise over 50 min and the reaction mixture was stirred at room temperature for 22 h. The mixture was diluted with water (130 mL) and washed with DCM (7 × 100 mL). The organic fractions were collected and washed further with water (2 × 100 mL), dried over $MgSO_4$, filtered, and concentrated under reduced pressure. DMF was removed by repeated distillation of the solution with toluene. The residue was purified by gravity column chromatography using 2:1 hexane/EtOAc as eluent. The product was obtained as a colorless oil in 86 % yield. The identity of the resulting product was confirmed by HR-MS (Fig. S2), ^{1}H NMR and ^{13}C NMR spectroscopy, and ATR-IR spectroscopy: ^{1}H NMR [34] (300 MHz, $CDCl_3$, 25 °C): δ (ppm) = 3.27–3.41 (m, 5H, –OC*H*$_3$, –OCH$_2$–C*H*$_2$–N$_3$), 3.48–3.55 (m, 2H, –OC*H*$_2$–CH$_2$–N$_3$, 3.57–3.68 (m, 12H, 3 × –OC*H*$_2$–C*H*$_2$O–); ^{13}C NMR [34] (75 MHz, $CDCl_3$, 25 °C): δ (ppm) = 72.1, 70.8, 70.8, 70.8, 70.8, 70.7, 70.2, 59.2, 50.8; ATR-IR [35,36] (cm^{-1}): 2870 (C–H str, aliphatic), 2098 (C–N$_3$), 1101 (C–O–C str).

2,5,8,11-Tetraoxatridecan-13-amine (mPEG$_4$-amine, **3**)

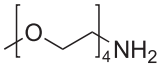

To a solution of **2** (3.0 g, 12.9 mmol, 1.0 eq.) in anhydrous THF (25 mL), triphenylphosphine (4.22 g, 16.1 mmol, 1.25 eq.) in anhydrous THF (15 mL) was added dropwise over 15 min under nitrogen atmosphere and the reaction mixture was stirred at room temperature for 5 h. Distilled water (20 mL) was then added, and the solution was refluxed for 22 h. The solution was concentrated under reduced pressure and the residue was purified by gravity column chromatography using 9:1 DCM/MeOH (+1% Et$_3$N). The product was obtained as a yellowish oil in 97 % yield. The identity of the resulting product was confirmed by HR-MS (Fig. S2), ^{1}H NMR and ^{13}C NMR spectroscopy, and ATR-IR spectroscopy: ^{1}H NMR [34] (300 MHz, $CDCl_3$, 25 °C): δ (ppm) = 2.82 (t, 2H, $^{3}J_{H-H}$ = 5.21 Hz, –CH$_2$–C*H*$_2$–NH$_2$), 3.33 (s, 3H, –OC*H*$_3$), 3.43–3.54 (m, 4H, –OCH$_2$–C*H*$_2$O–, –C*H*$_2$–CH$_2$–NH$_2$), 3.54–3.68 (m, 10*H*, 2 × –OC*H*$_2$–C*H*$_2$O, –OC*H*$_2$–CH$_2$O–); ^{13}C NMR (75 MHz, $CDCl_3$, 25 °C): δ (ppm) = 73.3, 72.1, 70.7, 70.7 (2 ×), 70.6, 70.4, 59.2, 41.8; ATR-IR [35,36] (cm^{-1}): 3372 (N–H str), 2866 (C–H str, aliphatic), 1100 (C–O–C str).

2.3. Size-exclusion chromatography (SEC)

SEC was employed to determine the molar-mass characteristics—namely, the number-average molar mass (M_n), weight-average molar mass (M_w), and dispersity ($Đ = M_w/M_n$)—of the synthesized polymers. For the parent polymer, DIBMA monomethyl ester, absolute molar-mass averages were determined using SEC coupled to a DAWN HELEOS II multi-angle light scattering (MALS) detector and an Optilab T-rEX refractive index (RI) detector (both from Wyatt Technology, USA). This setup, referred to as SEC–MALS–RI, allows for absolute molar-mass determination without reliance on calibration standards. Separation was performed at room temperature on an Agilent 1260 HPLC system (Agilent Technologies, USA) equipped with a TSKgel Alpha-2500 analytical column (7.8 mm x 300 mm, 7 μm) and a corresponding precolumn (both from Tosoh Bioscience, Japan). MeOH served as the mobile phase at a flow rate of 0.7 mL min^{-1}, and 100 μL MeOH containing 10 mg mL^{-1} DIBMA monomethyl ester was injected. The specific refractive index increment (d*n*/dc) of the polymer, necessary for absolute molar-mass calculations, was determined based on the injected mass and assuming complete mass recovery from the column. The absolute weight-average molar mass of DIBMA monomethyl ester was found to be M_w = 5.9 kg mol^{-1}, with a low dispersity of $Đ$ = 1.03. The SEC–MALS–RI chromatogram of the parent DIBMA monomethyl ester is provided in Fig. S3.

The functionalized polymers—Arg-DIBMA, Meg-DIBMA, Dab-DIBMA, and mPEG$_4$-DIBMA—were insoluble in MeOH; therefore, SEC measurements were conducted using an aqueous mobile phase comprising 50 mM Tris and 0.1 M NaCl at pH 8.0. These analyses were performed using SUPREMA 1000 Å and SUPREMA 50 Å columns (both 300 mm x 8 mm, 5 μm) along with a precolumn (all from PSS Polymer Standards Service, Germany). The columns were calibrated with polyacrylic acid (PAA; PSS Polymer Standards Service) standards possessing narrow molar-mass distributions. SEC chromatograms of Arg-DIBMA, Meg-DIBMA, Dab-DIBMA, and mPEG$_4$-DIBMA are presented in Fig. S4, with their relative molar-mass averages summarized in Table 1. All measurements were carried out at room temperature, and data acquisition and analysis were performed using ASTRA 7.3.1 software (Wyatt Technology).

2.4. Polymer stock solutions

Polymer powders used throughout this study were dissolved in 50 mM Tris-HCl or 50 mM HEPES, 200 mM NaCl unless noted otherwise, followed by incubation at 55 °C for 10–15 min with vortexing in an

Table 1
Molar-mass characteristics of functionalized DIBMA polymers determined by relative SEC with RI detection in 50 mM Tris and 0.1 M NaCl at pH 8.0, calibrated against PAA standards.

Polymer	M_n (kg mol^{-1})	M_w (kg mol^{-1})	$Đ$
Arg-DIBMA	2.3	6.0	2.6
Dab-DIBMA	2.6	18.8	7.2
Meg-DIBMA	2.4	6.5	2.7
mPEG$_4$-DIBMA	1.9	4.8	2.5

alternating fashion to yield a mass concentration of 50 mg/mL. The final pH value of polymer stock solutions was adjusted to 8.0 or 7.4, as indicated. All polymer stock solutions were then filtered through polycarbonate membranes with a pore size of 0.22 μm and stored at 4 °C.

2.5. Large unilamellar vesicles (LUVs)

DMPC powder was dissolved in 50 mM Tris-HCl or HEPES, 200 mM NaCl, pH 8.0 to a final concentration of 20 mg/mL. The lipid suspension was incubated at 35 °C for 30–40 min with vortexing every 10 min in an alternating fashion. In order to increase the hydration efficiency, the lipid suspension was then immersed in liquid nitrogen followed by thawing in a ThermoMixer (Eppendorf, Hamburg, Germany) at 35 °C for 5–10 freeze–thaw cycles. Subsequently, the DMPC suspension was loaded into gas-tight syringes and extruded at 35 °C through a 100-nm Whatman polycarbonate membrane filter at least 20 times using a Mini-Extruder (Avanti Polar Lipids, Alabaster, USA) to prepare LUVs.

2.6. Ultraviolet–visible (UV–vis) spectroscopy

The absorption spectra of polymers at 1 mg/mL dissolved in 50 mM Tris-HCl, 200 mM NaCl, pH 8.0 were recorded on a Jasco V-650 UV–vis spectrophotometer (Jasco, Groß-Umstadt, Germany). Measurements were performed at room temperature using a quartz cuvette with a 10-mm light path (Hellma Analytics, Müllheim, Germany) at a scan rate of 200 nm/min in the wavelength range of 220–600 nm.

2.7. Polymer-encapsulated lipid-bilayer nanodiscs

The DMPC LUVs suspension was added to the polymer stock solutions at different polymer/lipid mass ratios (m_P/m_L) and incubated at 35 °C for at least 16 h with shaking at 450 rpm to form polymer-encapsulated DMPC nanodiscs. All experiments were performed in aqueous buffer containing 50 mM Tris-HCl, 200 mM NaCl, pH 8.0.

2.8. Dynamic light scattering (DLS)

Solubilization efficiencies of all polymers were confirmed and quantified with the aid of DLS using DMPC model membranes. A Zetasizer Nano S (Malvern Panalytical, Malvern, UK) was used to perform DLS measurements in a 70-μL microcuvette (Brand, Wertheim, Germany) at a temperature of 25 °C. The DLS instrument was equipped with a He–Ne laser having a wavelength of 633 nm, and the detection scattering angle was 173°. The sample was thermostatted for 5 min at 35 °C prior to measurement.

2.9. Differential scanning calorimetry (DSC)

DSC measurements were carried out using a MicroCal VP-DSC calorimeter (Malvern Panalytical, Malvern, UK) to monitor the thermotropic behavior of DMPC lipids in the absence and presence of polymers. Samples were prepared in 50 mM Tris-HCl, 200 mM NaCl, pH 8.0 at various m_P/m_L values. Polymer/DMPC samples and reference buffer were first degassed and then measured in 5–10 heating and cooling cycles at a scan rate of 60 °C h^{-1} in the range of 2–80 °C. One representative curve was chosen from the closely overlaid scan traces, the buffer baseline was subtracted, and the data were normalized against the DMPC concentration (6 mM) using MicroCal Origin 7.0 software (OriginLab, Northampton, USA). The phase transition temperature (T_m) was determined as the temperature at which the excess molar isobaric heat capacity (C_p) reached its maximum value. The size of the cooperative unit (CU) was obtained as the ratio of the van't Hoff enthalpy, given by the shape of the melting peak, to the calorimetric enthalpy, given by the peak area [37].

2.10. Turbidity experiments

The colloidal stability of $mPEG_4$-DIBMA lipid particles in the presence of divalent cations was evaluated with turbidity experiments at 620 nm using a Tecan Spark 10 M microplate reader (Tecan, Männedorf, Switzerland).

2.11. ζ-potential measurements

Samples containing 4 mg/mL DMPC LUVs, 8 mg/mL polymer, or polymer/DMPC nanodiscs at $m_P/m_L = 2$ were prepared in 50 mM Tris-HCl, 100 mM NaCl, pH 7.4. ζ-potential measurements were carried out on a Zetasizer Nano ZS (Malvern Panalytical, Malvern, UK) using disposable folded capillary zeta cells DTS1070 (Malvern Panalytical, Malvern, UK) at a detection scattering angle of 173° and a temperature of 25 °C. The diffusion barrier technique was used to prepare the sample cell for ζ-potential measurement [38]. The folded capillary cell was first filled with buffer before 100 μL of sample was pipetted directly into the cell bottom with the aid of a gel-loading tip, avoiding mixing of the sample with buffer during loading. The cell was capped and equilibrated for 300 s prior to measurement to reduce fluid motion induced by temperature gradients.

2.12. Adrenocorticotropic hormone peptide (ACTH)

The truncated human ACTH construct ACTH(1–23)Cys was subcloned into a pET-16b vector, including a 6xHis tag at the N-terminus, followed by a B1 domain of streptococcal protein G (GB1 fusion protein) and a tobacco etch virus (TEV) cleavage site. *Escherichia coli* BL21 (DE3) cells were used for peptide expression. Cells were cultured in 2xYT medium at 37 °C, 140 rpm in baffled flask, supplemented with 100 μg/mL ampicillin. The expression was inducted with 1 mM isopropyl-β-D-thiogalactopyranoside (IPTG) upon the optical density 600 (OD_{600}) reached 0.6–0.8. Cells were harvested by centrifugation at 6,000 *g*, 10 min, 4 °C after 5 h induction, flash-frozen in N_2 (l), and stored at −80 °C for future use. Cell pellets were resuspended in lysis buffer containing 50 mM sodium phosphate, pH 7.5, 300 mM NaCl, 1 mM dithiothreitol (DTT), supplemented with EDTA free cOmplete protease inhibitor cocktail tablet (Roche). The homogenate was sonicated on ice, and the lysate was centrifuged at 100,000 *g* for 25 min at 4 °C. The supernatant was incubated with Ni-NTA resin (Macherey-Nagel, Düren, Germany) at 4 °C overnight with gentle rotation. The resin was loaded onto a gravity column and washed with 10 column volumes (CVs) lysis buffer and 10 CVs lysis buffer supplemented with 20 mM imidazole. The peptide was eluted with 10 CVs lysis buffer supplemented with 250 mM imidazole. Fractions containing peptides were collected and dialyzed against lysis buffer using 3.5 K MWCO SnakeSkin dialysis tubing (Thermo Fisher Scientific, Dreieich, Germany) at 4 °C overnight. The fusion protein was removed by addition of home-made TEV protease. The cleaved peptide was further purified by size-exclusion chromatography (Superdex 16/600, 30 pg column; GE Healthcare, München, Germany) with a running buffer containing 20 mM ammonium bicarbonate. Peptide labeling with thiol-reactive ATTO-488 maleimide (ATTO-TEC, Siegen, Germany) was carried out according to the manufacturer's instructions. The labeled peptide was further purified using high-performance liquid chromatography (HPLC) using a Zorbax SB300 C8 4.6 × 250 mm analytical column (Agilent Technologies, Waldbronn, Germany).

2.13. Microfluidic diffusional sizing (MDS)

ATTO 488-labeled human ACTH peptide was added to polymer/DMPC nanodiscs at $m_P/m_L = 4$ to a final peptide concentration of 20 nM. The final concentration of DMPC was 4 mg/mL. Interactions between peptide and polymer/DMPC nanodiscs were measured on a Fluidity One-W system (Fluidic Analytics, Cambridge, UK) by recording changes in hydrodynamic particle size [39,40]. Disposable MDS chips were used

holding a total sample volume of 5 μL. All experiments were carried out in 50 mM HEPES, 200 mM NaCl, pH 7.4 or 8.0.

2.14. Negative-stain transmission electron microscopy (TEM)

TEM specimens were prepared by spreading 4 μL mPEG$_4$-DIBMA/DMPC nanodiscs at m_P/m_L = 4 onto freshly glow-discharged copper grids (15 mA for 25 s at 0.39 mbar) coated with a carbon support film. Excess suspension was blotted off after ~5 s using filter paper. Grids were washed with 5 μL MilliQ water once, followed by staining with 5 μL 2 % (*w/v*) aqueous uranyl acetate solution twice and blotted off after ~15 s with filter paper. After preparation, specimens were air-dried and examined on a Talos L120C transmission electron microscope equipped with a 4 k × 4 K Ceta CMOS camera (Thermo Fisher Scientific, Dreieich, Germany).

2.15. Preparation of insect membranes and solubilization of MC$_4$R

Wild-type MC$_4$R (UniProtKB-P32245) was codon-optimized and inserted into a mortified pFastbac1 vector, including an influenza virus hemagglutinin (HA) signal peptide followed by a Flag tag at the N-terminus as well as a human rhinovirus (HRV3C) cleavage site and a 10xHis tag at the C-terminus by using NcoI-EcoRI restriction endonucleases (New England Biolabs, Ipswich, USA). The thermostabilized mutant MC$_4$R construct was modified by introducing 5 mutations (E49$^{1.37}$V, N97$^{2.57}$L, S99$^{2.59}$F, S131$^{3.34}$A and D298$^{7.49}$N, where superscript numbers correspond to the Ballesteros–Weinstein nomenclature [41]) containing the same tags as the wild type, a generous gift of Prof. Dr. Raymond C. Stevens (iHuman Institute, ShanghaiTech University, China) [42]. The MC$_4$R–eYFP construct was modified by introducing the eYFP gene between the HRV3C cleavage site and the 10xHis tag. Recombinant baculovirus production of MC$_4$R–eYFP was generated by transfecting *Spodoptera frugiperda* (Sf9) cells grown in Sf-900 III SFM media (Thermo Fisher Scientific, Dreieich, Germany) at 27 °C with Bacmid (Bac-to-Bac system, Thermo Fisher Scientific, Dreieich, Germany) using FuGENE HD transfection reagent according to the manufacturer's instructions. Sf9 cells were infected at a density of 2 to 3 × 10^6 cells/mL with recombinant baculovirus. 72 h after infection, cells were harvested by centrifugation at 6,000 *g*, 4 °C for 10 min and stored at −80 °C. Cellular membranes were prepared as described previously with slight modifications [42]. In brief, Sf9 cell pellets were resuspended in a hypotonic buffer containing 10 mM HEPES, 10 mM $MgCl_2$, 20 mM KCl, pH 7.8 and cOmplete EDTA-free protease inhibitor cocktail tablet (Roche, Basel, Switzerland) and then lysed by sonication on ice (Sonorex; Bandelin, Berlin, Germany). Cell membranes containing MC$_4$R–eYFP were harvested by ultracentrifugation at 120,000 *g*, 4 °C for 30 min (Optima xpn-80 ultracentrifuge, Beckman Coulter, Brea, USA). The membrane pellet was resuspended in the same hypotonic buffer and disrupted with a Dounce homogenizer followed by ultracentrifugation at 120,000 *g*, 4 °C for 30 min. The above procedure was repeated twice. Further membrane purification was performed three times using hypotonic buffer supplemented with 1 M NaCl. Purified membrane pellets were washed once with 50 mM HEPES, 200 mM NaCl, pH 8.0, flash-frozen in liquid nitrogen, and stored at −80 °C. Polymers were added to 20 mg/mL (wet mass/volume) purified cellular membranes at different concentrations and incubated at 4 °C for either 4 h or 16 h with gentle rotation. Supernatants were collected after ultracentrifugation at 120,000 *g*, 4 °C for 30 min. Western blot analysis was carried out using membrane preparations and polymer solubilization as described above. The buffer contained 200 mM NaCl and 50 mM HEPES at pH 8.0 or pH 7.5 for SMA(2:1) and was supplemented with 2.5 % (*w/v*) of the indicated polymers. The thermostabilized MC$_4$R construct used for crystallographic studies (construct C5 in Ref. [42]) was employed, which did not include the eYFP tag. Detection was performed using a monoclonal anti-FLAG antibody (F1804; Sigma–Aldrich, Darmstadt, Germany). For NaCl screening, 2.5 % (*w/v*) polymer and 50 mM HEPES pH 8.0 were supplemented with the indicated concentrations of NaCl. Data were referenced to the DDM/CHS signal running on the same gel and normalized.

3. Results and discussion

3.1. Design, synthesis, and characterization of copolymers

The goal of our synthetic approach was to reduce the charge density on the polymer backbone by derivatizing DIBMA through amidation of one of the two carboxylic acid groups in each repeating unit (Scheme 1). We have previously used the same strategy to produce Glyco-DIBMA, which offers several advantages over unmodified DIBMA, including a higher protein-extraction efficiency [32,33]. Here, we sought to explore a larger chemical space through amidation using a set of structurally diverse amines, including: α-amino acids such as L-arginine (Arg) and L-2,4-diaminobutyric acid (Dab); the hexosamine meglumine (Meg); and the oligo (ethylene oxide) tetraethyleneglycol monomethyl ether amine (mPEG$_4$). These compounds have in common that they contain at least one reactive amino group, are highly water-soluble, biocompatible, and net neutral once coupled to the polymer backbone through an amide linkage. We considered these properties important to reduce the charge density on the DIBMA polymer backbone while retaining its excellent water solubility. Four polymers were thus synthesized, henceforth referred to as Arg-DIBMA, Dab-DIBMA, Meg-DIBMA, and mPEG$_4$-DIBMA.

Quantitative determination of the degrees of functionalization via NMR spectroscopy was impeded by partial overlap between polymer backbone signals and those of the functional groups (Fig. S1, left). While ATR-IR spectroscopy suggested high levels of functionalization (Fig. S1, right), it is inherently a qualitative technique. Despite the possibility of partial functionalization—a common outcome in post-polymerization modifications due to kinetic and steric constraints—the achieved functionalization was sufficient to render the polymers water-soluble, unlike the parent DIBMA monomethyl ester. This solubility enhancement, coupled with improved performance metrics such as efficient lipid extraction, nanodisc formation, reduced nonspecific ligand interactions, and enhanced GPCR extraction efficiency (*vide infra*), underscores the practical utility of these polymers in GPCR research.

To assess the molar-mass characteristics and structural homogeneity of the synthesized polymers, SEC analyses were conducted (Table 1). The parent DIBMA monomethyl ester exhibited a narrow molar-mass distribution with a low dispersity of 1.03 when analyzed via SEC coupled with MALS and RI detection (SEC–MALS–RI) in MeOH (Fig. S3). In contrast, the functionalized DIBMA variants—Arg-DIBMA, Meg-DIBMA, Dab-DIBMA, and mPEG$_4$-DIBMA—were insoluble in MeOH

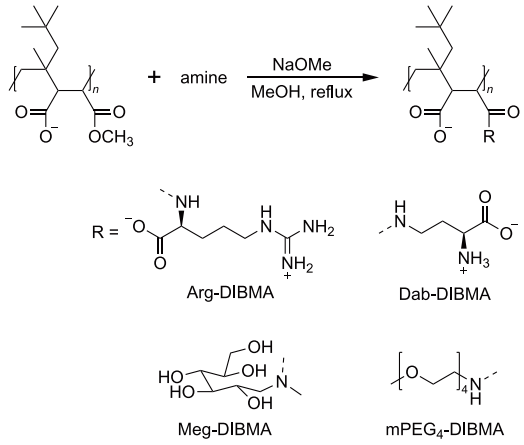

Scheme 1. General scheme for the synthesis of DIBMA-based amphiphilic copolymers that form lipid-bilayer nanodiscs.

and thus analyzed using conventional SEC with RI detection (SEC–RI) in aqueous buffer, employing PAA standards for column calibration. Because of these different solvents and calibration methods, the M_n values of the parent and modified polymers cannot be quantitatively compared. We therefore focus on dispersity ($Đ$), which consistently increased upon functionalization, reflecting heterogeneous side-group attachment and possible associative behavior of less-modified chains in aqueous solution. Nevertheless, all functionalized polymers displayed unimodal SEC–RI elution profiles (Fig. S4), albeit with higher dispersities compared to the parent polymer (Table 1). This increase in dispersity is attributed to variations in the degree of functionalization with bulky side groups, which influence the hydrodynamic volume. In addition, polymer chains with lower degrees of functionalization may exhibit associative behavior in aqueous environments, given the inherent insolubility of the unmodified parent polymer. Nonetheless, the observed water solubility of the modified polymers confirms successful functionalization, reinforcing their suitability for biophysical and biochemical applications.

3.2. Nanodisc-forming properties

Each polymer variant was subsequently tested for its key biophysical and nanodiscs-forming properties, including lipid extraction from synthetic vesicles as well as protein extraction from eukaryotic cells. First, we investigated the formation of polymer/DMPC nanodiscs and the solubilization efficiency of the new polymers. To this end, LUVs made from DMPC were incubated with each polymer at different polymer/lipid mass ratios, and particle size distributions were analyzed by DLS. At $m_P/m_L = 2.0$, the hydrodynamic particle sizes of all new nanodiscs were in the expected range of ~10 nm (Fig. 1a). By contrast, at a lower m_P/m_L of 0.5, substantial differences in hydrodynamic particle sizes were observed, reflecting differences in the solubilization efficiency among the polymers (Fig. 1b). A more systematic screening of polymer/lipid mass ratios revealed that, at $m_P/m_L \geq 1$, all new polymers formed smaller and more well-defined nanodiscs compared with DIBMA (Fig. 1a and c). These nanodiscs consistently exhibited hydrodynamic diameters of ~10 nm and narrow size distributions (Fig. 1c). This property is particularly beneficial for structural studies by cryogenic electron microscopy (cryoEM) and NMR spectroscopy, where sample homogeneity is important.

Consequently, a polymer/lipid mass ratio of 1 or higher should be used for all new DIBMA variants to obtain the often-desired nanodisc diameter of ~10 nm (Fig. 1c, upper panel). This minimal m_P/m_L ratio is considerably less than that required for unmodified DIBMA but is about twice as large as for SMA(2:1) and Sulfo-DIBMA (Fig. 1c, lower panel). Sulfo-DIBMA, a recent electroneutral DIBMA variant, contains an imide ring [34], in contrast with the open amide linkage of the DIBMA variants reported here (Scheme 1). In the above solubilization experiments, we focused on DMPC as a model lipid to assess the general feasibility of assembling lipid-bilayer nanodiscs under defined *in vitro* conditions and to further identify potential unspecific interactions of the respective polymers with the ACTH peptide (*vide infra*). Previous studies [43] on other polymers using more complex lipid mixtures suggest that the new polymers presented here will also be applicable to the *in vitro* assembly of nanodiscs comprising a broader range of lipids. This is corroborated by our finding that all new polymers effectively solubilize heterogenous native membranes and extract membrane proteins from them (*vide infra*).

3.3. Suitability for interaction studies

Next, we tested the suitability of each new polymer for characterizing interactions that are susceptible to charge effects. Most existing polymers, such as SMA and DIBMA, are incompatible with ligand binding assays for various GPCRs because of unspecific interactions between the polyanionic polymer chains and the ligands [44]. To assess the new DIBMA variants for their suitability in such ligand binding studies, we performed MDS measurements with the binding fragment of ACTH, a potent agonist of MC_4R [45]. MDS allows for the determination of the hydrodynamic particle size of bare ACTH and its increase resulting from unspecific interactions with nanodiscs [39,40]. To evaluate the interactions between the DIBMA variants and ACTH, we used polymer-encapsulated nanodiscs containing the zwitterionic phospholipid DMPC, a lipid known not to interact with ACTH [44]. Polymer/DMPC nanodiscs were prepared at $m_P/m_L = 4$ to obtain small nanodiscs, as confirmed by DLS (Fig. 1c and Fig. S5). In line with previous

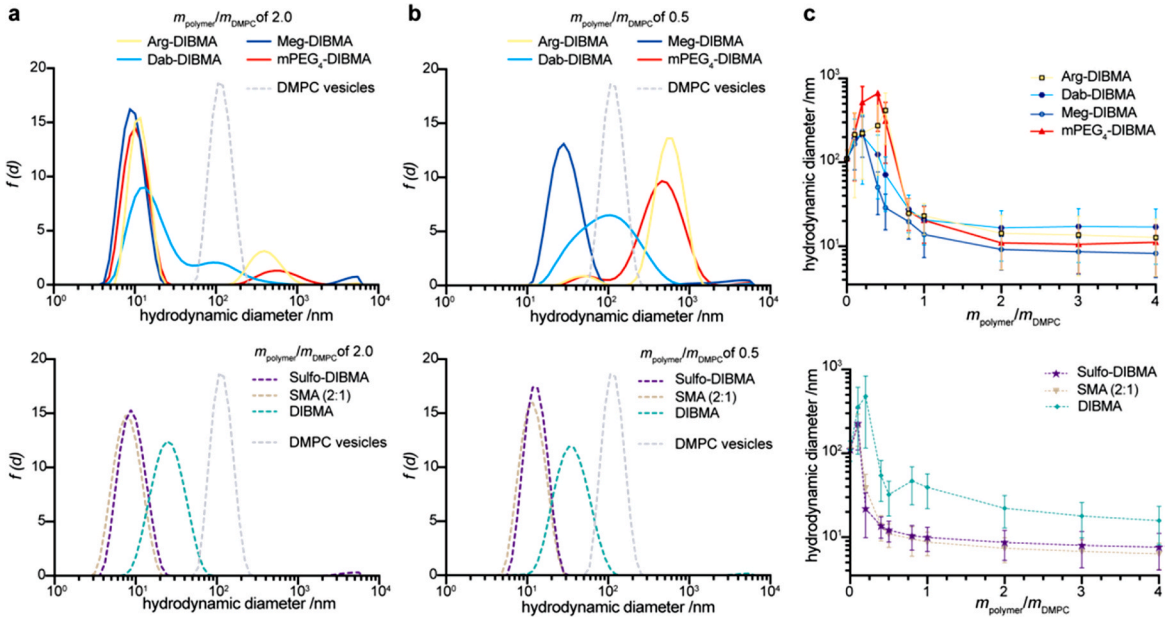

Fig. 1. Particle size analysis shows formation of homogenous nanodiscs for all polymers at polymer/lipid mass ratios >1. (a and b) Intensity-weighted particle size distributions of mixtures containing polymer and DMPC (4 mg/mL) at polymer/lipid mass ratios of (a) 2.0 and (b) 0.5 as obtained from DLS. Upper panels show data for the new DIBMA variants, while lower panels serve as reference for established polymers. (c) *z*-Average particle diameters derived from DLS as functions of the polymer/DMPC mass ratio, m_P/m_L. Vertical bars indicate size distribution widths defined as $\sigma = z\sqrt{PDI}$, where PDI is the polydispersity index.

observations [44], our MDS results confirmed that the hydrodynamic particle size of ACTH remained unchanged upon addition of DMPC nanodiscs encapsulated by the electroneutral polymer Sulfo-DIBMA, indicating the absence of unspecific interactions between the polymer and the ligand (Fig. 2). In contrast with Sulfo-DIBMA, we observed an increase in hydrodynamic particle size when ACTH was exposed to nanodiscs encapsulated by DIBMA, Arg-DIBMA, Dab-DIBMA, or Meg-DIBMA, suggesting unspecific interactions between the cationic peptide ligand and the anionic polymers. In stark contrast, the hydrodynamic particle size of ACTH remained unchanged upon addition of nanodiscs encapsulated by the PEGylated polymer mPEG$_4$-DIBMA, even though mPEG$_4$-DIBMA still carries carboxylate groups (Scheme 1). For all polymers, the same interaction behaviors were found at two different pH values (pH 7.4, Fig. 2 and pH 8.0, Fig. S6), confirming that mPEG$_4$-DIBMA is of particular interest for studying the specific binding of ligands to nanodiscs-embedded membrane proteins under commonly applied buffer conditions.

3.4. Physicochemical properties of mPEG$_4$-DIBMA

Due to its promising features in ligand-binding assays, we carried out a more comprehensive characterization of mPEG$_4$-DIBMA. First, we investigated the origin of the reduced unspecific interactions with ACTH by determining the ζ-potential. Our results confirmed that unmodified DIBMA indeed has a strongly negative ζ-potential, which is only partly reduced by the mPEG$_4$ modification, in contrast with electroneutral Sulfo-DIBMA (Fig. 3a). Negative ζ-potentials were similarly detected in lipid-free polymer samples and for lipid-encapsulating nanodiscs. From this finding, we infer that unspecific binding to mPEG$_4$-DIBMA is not prevented by a lack of charged groups on the polymer but rather by the relatively bulky, strongly hydrated PEG chains, which sterically block access of the peptide to the polymer backbone. This interpretation is consistent with the expected Debye–Hückel screening length of <1 nm under the applied conditions, suggesting, that the unspecific interactions between the positively charged peptide and the negatively charged carboxylate groups are much less prominent in mPEG$_4$-DIBMA because of their spatial separation by the hydrated PEG chains and the shielding effects of the buffer ions. Importantly, we chose to use short PEG chains containing only four oxyethylene units. These short PEG chains are designed to prevent unspecific interactions of cations with the negatively charged polymer backbone while avoiding interference with

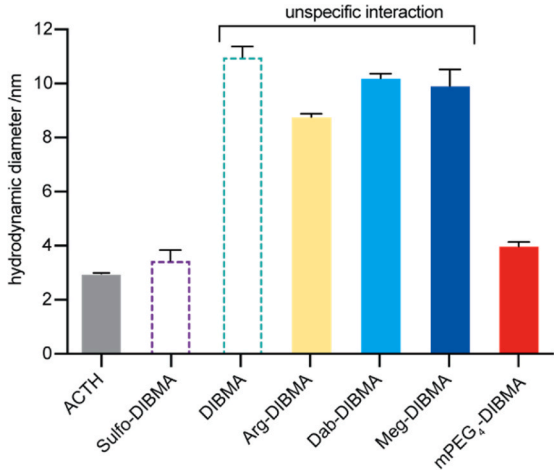

Fig. 2. Only mPEG$_4$-DIBMA shows reduced unspecific interactions with the cationic peptide ligand ACTH. Unspecific interactions between ACTH and polymer/DMPC nanodiscs at $m_P/m_L = 4$ were measured by means of MDS. All experiments were carried out at 50 mM HEPES, 200 mM NaCl, pH 7.4. Error bars represent one standard deviation of two independent experiments, each repeated in triplicate.

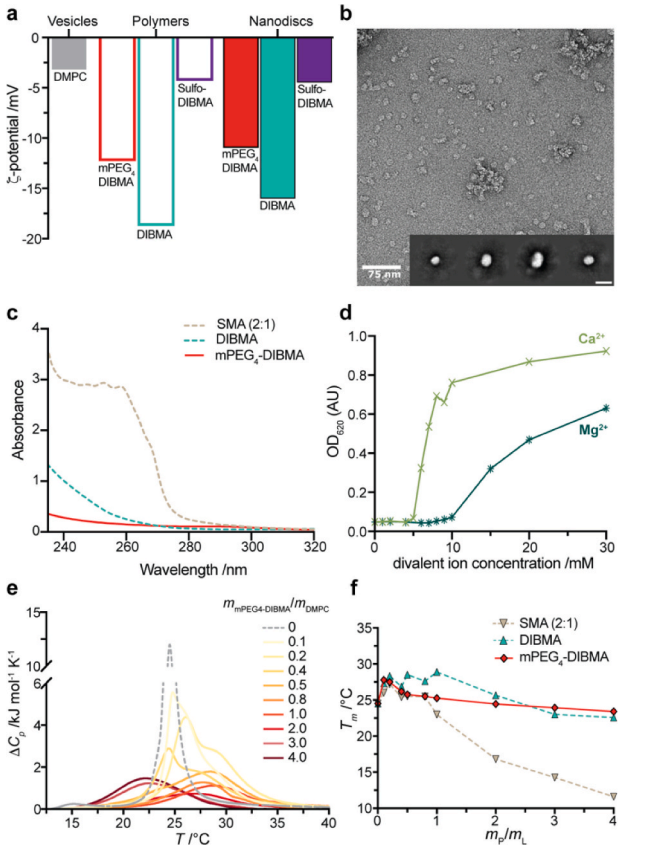

Fig. 3. Physicochemical properties of mPEG$_4$-DIBMA. (a) ζ-potentials of mPEG$_4$-DIBMA, DIBMA, Sulfo-DIBMA, and respective polymer-encapsulated DMPC nanodiscs. (b) Negative-stain TEM image of mPEG$_4$-DIBMA/DMPC nanodiscs at $m_P/m_L = 4$. Insert shows 2D class averages of auto-picked particles from a total of 18 micrographs (scale bar: 10 nm). (c) UV absorption spectra of mPEG$_4$-DIBMA, DIBMA, and SMA(2:1). (d) Colloidal stability of mPEG$_4$-DIBMA/DMPC nanodiscs at $m_P/m_L = 4$ as determined by turbidity in response to increasing concentration of Mg^2 or Ca^{2+}. (e) DSC thermograms displaying the excess molar isobaric heat capacities (ΔC_p) of 4 mg/mL DMPC LUVs and mPEG$_4$-DIBMA/DMPC nanodiscs at the indicated polymer/DMPC mass ratios, m_P/m_L. (f) Main phase transition temperature (T_m) as a function of the polymer/DMPC mass ratio, m_P/m_L.

protein–protein and protein–ligand interactions of encapsulated membrane proteins.

Next, we assessed the morphology of mPEG$_4$-DIBMA/DMPC nanodiscs with the aid of negative-stain TEM. TEM micrographs and 2D classifications of auto-picked particles demonstrated the presence of homogeneously sized nanodiscs with an average diameter of ~10 nm (Fig. 3b), consistent with our DLS data (Fig. 1). Furthermore, absorbance measurements showed that mPEG$_4$-DIBMA has a very low absorbance in the ultraviolet (UV) spectral range, offering favorable properties for the photometric quantification of protein levels (Fig. 3c). To evaluate the effects of divalent cations on the colloidal stability of nanodiscs, we measured the turbidity of mPEG$_4$-DIBMA/DMPC nanodiscs as a function of increasing Mg^{2+} or Ca^{2+} concentrations. mPEG$_4$-DIBMA/DMPC nanodiscs began to precipitate at divalent cation concentrations of 10 mM Mg^{2+} or 5 mM Ca^{2+} (Fig. 3d and Fig. S7). For comparison, polyanionic SMA and DIBMA polymers precipitate in the presence of 2 mM and >20 mM divalent cations [27], respectively, whereas electroneutral Sulfo-SMA and Sulfo-DIBMA remain soluble even at 80 mM divalent cations [44]. Thus, mPEG$_4$-DIBMA/DMPC nanodiscs exhibit a rather modest colloidal stability in the presence of divalent cations, as expected for negatively charged nanodiscs. Nevertheless, this modest stability is still sufficient for physiological concentrations of divalent cations and

should, therefore, support activity studies of membrane proteins requiring typical divalent cation concentrations.

To investigate the integrity of the nanodisc's lipid matrix, we measured the effect of mPEG$_4$-DIBMA on the thermotropic behavior of the encapsulated lipid-bilayer patch using DSC. DSC thermograms showed that the phase-transition peak became broader with increasing m_P/m_L (Fig. 3e). This observation confirms the formation of smaller lipid-bilayer nanoparticles upon addition of mPEG$_4$-DIBMA to DMPC vesicles, which showed the expected highly cooperative gel-to-fluid transition at ~24.5 °C (Fig. 3e, grey). It is worth noting that multiple phase transition peaks were observed at low polymer/lipid mass ratios, where nanodiscs coexist with vesicles (Fig. 3e and Fig. S8). Hence, it appears that a polymer/lipid mass ratio of ~1 is required for mPEG$_4$-DIBMA to fully solubilize DMPC vesicles, in agreement with our DLS data (Fig. 1c) and in contrast with SMA(2:1) (Fig. 3e and Fig. S8a). At higher polymer/lipid ratios, the mPEG$_4$-DIBMA nanodiscs revealed a moderate decrease in the phase transition temperature (T_m) to about 22 °C. We infer that the DMPC molecules along the perimeter of the nanodiscs were affected by mPEG$_4$-DIBMA, whereas the core of the DMPC bilayer in the nanodiscs was not significantly affected. Similar results were observed in DSC measurement of DIBMA/DMPC nanodiscs (Fig. 3f and Fig. S8b), in line with previous findings [27]. In contrast, SMA-encapsulated nanodiscs showed a steep drop in T_m with increasing polymer concentration down to 11.6 °C at $m_P/m_L = 4$ (Fig. 3f and Fig. S8a). This observation has been explained by a perturbation of the lipids' acyl chain packing by the polymer, which might be caused by the intercalation of the phenyl groups of SMA(2:1) [46]. Overall, our DSC data demonstrate that, in comparison with SMA(2:1), mPEG$_4$-DIBMA requires slightly elevated polymer/lipid mass ratios for complete solubilization. However, mPEG$_4$-DIBMA also has much milder effects on the lipid matrix under the conditions required to prepare small and homogenous nanodiscs, making it an ideal tool for subsequent biophysical or structural studies.

3.5. Extraction capabilities of GPCRs from insect cell membranes

In addition to solubilizing synthetic lipids, we tested the capacities of all new polymers to extract and encapsulate integral transmembrane proteins from cellular membranes into nanodiscs. For this purpose, we selected a prototypical GPCR, specifically a thermostabilized MC$_4$R mutant (MC$_4$R–eYFP) carrying an enhanced yellow fluorescent protein (eYFP) tag [42]. We exposed crude membrane preparations from Sf9 insect cells to different polymer concentrations and quantified the amounts of extracted MC$_4$R by measuring the emission intensities of eYFP (Fig. 4). Notably, all four new DIBMA variants considerably enhanced the solubilization efficiency compared with unmodified DIBMA (Fig. 4). Similar results were obtained from quantitative western blot analyses using an MC$_4$R construct that does not include the eYFP tag (Fig. S9). These data (i) provided independent validation of the enhanced solubilization capabilities of the new polymers compared with unmodified DIBMA (Fig. S9a and b); (ii) allowed for the exclusion of potential artifacts introduced by the eYFP-fusion construct (Fig. S9a and b); and (iii) enabled more reliable screening of ion concentrations, which would affect eYFP fluorescence (Fig. S9c–f). Previous findings have shown that DIBMA carries higher negative charge densities than SMA(2:1) under similar conditions [28]. As a result, strong Coulombic repulsion may affect the interaction of DIBMA with the negatively charged cell membrane and hinder the extraction of membrane proteins into native nanodiscs.

Our data show that the newly designed DIBMA variants indeed facilitate the cell-membrane fragmentation process, resulting in higher extraction efficiencies. With the exception of Dab-DIBMA, all new DIBMA variants also offered solubilization efficiencies comparable to or surpassing that of SMA(2:1) at polymer concentrations ≥1 %. Again, mPEG$_4$-DIBMA displayed the best performance, approaching solubilization yields similar to the DDM/CHS system that was used as reference

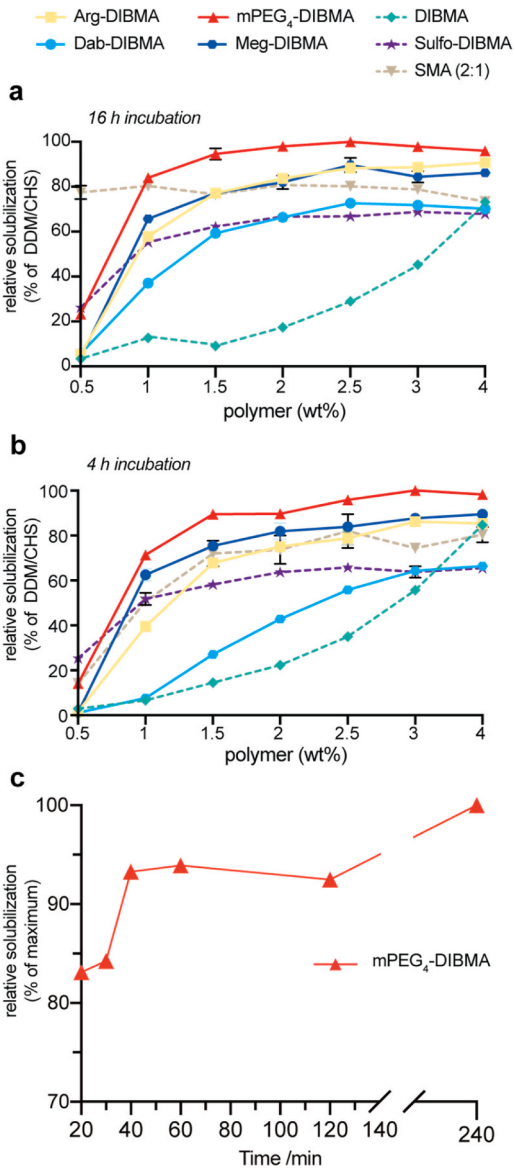

Fig. 4. All new DIBMA variants, in particular mPEG$_4$-DIBMA, efficiently extract the GPCR MC$_4$R. (a and b) Polymer-mediated extraction of MC$_4$R–eYFP from insect membranes. The extraction efficiencies of the different polymers in comparison with the frequently used DDM/CHS system (1 % (*w/v*) DDM and 0.2 % (*w/v*) cholesteryl hemisuccinate (CHS)) are plotted. The amount of solubilized MC$_4$R for each preparation was determined by eYFP fluorescence after incubation with the indicated polymers for either (a) 16 h or (b) 4 h. (c) Normalized solubilization efficiency of 2 % (*w/v*) mPEG$_4$-DIBMA as a function of incubation time.

and generally serves as a gold standard for the extraction of GPCRs. In direct comparison with electroneutral Sulfo-DIBMA, the solubilization of MC$_4$R was about 1.5-fold higher with mPEG$_4$-DIBMA, making this new DIBMA variant particularly interesting for studies where the amount of extracted membrane protein is a limiting factor. While reliable functional characterization of the extracted MC$_4$R was not attempted here due to the limited quantities of the newly synthesized polymers, we observed native-like ligand-binding features for the MC$_4$R extracted via Sulfo-DIBMA (manuscript in preparation). This suggests that MC$_4$R maintains its function after extraction into polymer-encapsulated native nanodiscs. Noteworthily, many functional and structural studies of GPCRs suffer from limited stability of these labile receptors. Therefore, long incubation times of the cell pellet with the polymer may adversely affect subsequent *in vitro* studies. To address this

important point, we lastly tested the effects of reducing the incubation time (Fig. 4b, 4 h). These data largely reproduced the results obtained at longer incubation times (Fig. 4a, 16 h). The only exceptions were SMA (2:1) and Dab-DIBMA at low polymer concentrations, which displayed significantly lower extraction efficiencies at 4 h than at 16 h incubation. A more thorough analysis carried out for $mPEG_4$-DIBMA further suggested that even shorter incubation times, in the range of 20–60 min, can be used to efficiently extract MC_4R (Fig. 4c).

Taken together, we found that all new DIBMA variants can solubilize synthetic lipids and extract a prototypical GPCR from insect cells into native nanodiscs. Despite the advantages of native membrane extraction, it is important to note that polymer-based extraction strategies are often specific to the cell type and membrane protein. Therefore, the results presented here may not be directly transferable to other cell and protein systems. Furthermore, native nanodiscs exhibit increased heterogeneity compared to MSP nanodiscs and may display variable polymer/lipid ratios, destabilizing effects at the polymer–lipid interface, and potential unspecific interactions between polymers and proteins. Nevertheless, our MDS assay identified $mPEG_4$-DIBMA as a new member of the small set of polymers that avert unspecific Columbic interactions with a cationic peptide ligand, thus facilitating interaction studies using nanodisc-embedded membrane proteins. Furthermore, we observed outstanding performance of $mPEG_4$-DIBMA in efficiently extracting MC_4R from cellular membranes. Paired with its decent Mg^{2+} and Ca^{2+} tolerance and its low UV absorbance, $mPEG_4$-DIBMA shows particularly high potential for future applications in membrane-protein research.

4. Conclusions

Polymer-encapsulated nanodiscs offer several advantages over other membrane mimetics, including the detergent-free extraction of target membrane proteins while maintaining their native lipid-bilayer environment. Various amphiphilic copolymers, such as SMA and DIBMA, have been successfully used for purifying membrane proteins from different cells and determining membrane-protein structures [31,47–49]. Moreover, a diverse set of nanodisc-forming polymers with improved properties has been derived from SMA through amidation [50–53], imidation [51,54], or esterification [55]. In general, these polymers vary in key features such as extraction efficiency, tolerance to divalent metal ions, UV absorbance, and charge density—factors that often limit interaction studies using polymer-encapsulated nanodiscs. Although all of these properties are essential for characterizing membrane proteins such as GPCRs, none of the currently available polymers combine all the desirable features, necessitating compromises during the selection process. To overcome this limitation, we have introduced and tested a series of new DIBMA variants. All the new polymers show promising characteristics, particularly in terms of their efficiencies in extracting a GPCR from insect membranes. Among them, a PEGylated polymer, $mPEG_4$-DIBMA, emerged as the top performer across all tested properties. $mPEG_4$-DIBMA overcomes some of the significant limitations of SMA and DIBMA without compromising protein yields, highlighting its potential for the functional and structural characterization of membrane proteins within their native lipid-bilayer environment.

Author contributions

CC carried out biophysical and cell biology experiments; SS recorded and analyzed EM data; CV and SK designed polymers; CV and MCB synthesized polymers; GNR performed and analyzed HR-MS experiments; DP and EZ carried out SEC analyses, evaluation, and interpretation; ME, SK, and GFS designed, supervised, and discussed experiments; CC, CV, SK, and ME wrote the manuscript. All authors contributed to data analysis, scientific discussions, and content of the manuscript.

Declaration of competing interest

The authors declare that they have no known competing financial interests or personal relationships that could have appeared to influence the work reported in this paper.

Acknowledgements

We thank Prof. Dr. Georg Groth (Heinrich Heine University, Düsseldorf, Germany) for granting access to a DLS instrument, Prof. Dr. Raymond C. Stevens and Jing Yu (iHuman Institute, ShanghaiTech University, China) for providing us with a plasmid encoding the thermostabilized MC_4R, and Sarah Tutz (University of Graz, Austria) for excellent technical assistance. This work was supported by the German Research Foundation (DFG) (ET 103/4-1, ET 103/4-3, and the Heisenberg grant ET 103/5-1) to M.E. and the CSC (No. 201708320246) to C.C. This research was funded in whole, or in part, by the Austrian Science Fund (FWF) [grant DOI 10.55776/I5359 to S.K.]. For the purpose of open access, the author has applied a CC BY public copyright licence to any Author Accepted Manuscript version arising from this submission.

Appendix A. Supplementary data

Supplementary data to this article can be found online at https://doi.org/10.1016/j.ymeth.2025.08.013.

Data availability

Data will be made available on request.

References

[1] X. Zhang, S. Dong, F. Xu, Trends Biochem. Sci 43 (2018) 1033–1046.
[2] R.G. MacKenzie, Peptides 27 (2006) 395–403.
[3] J. Zhao, Y. Deng, Z. Jiang, H. Qing, Front. Aging Neurosci. 8 (2016) 1–15.
[4] T.H. Bayburt, Y.V. Grinkova, S.G. Sligar, Nano Lett. 2 (2002) 853–856.
[5] S. Inagaki, R. Ghirlando, J.F. White, J. Gvozdenovic-Jeremic, J.K. Northup, R. Grisshammer, J. Mol. Biol. 417 (2012) 95–111.
[6] D.Y. Zhao, M. Pöge, T. Morizumi, S. Gulati, N. Van Eps, J. Zhang, P. Miszta, S. Filipek, J. Mahamid, J.M. Plitzko, W. Baumeister, O.P. Ernst, K. Palczewski, J. Biol. Chem. 294 (2019) 14215–14230.
[7] J. Oates, A. Watts, Curr. Opin. Struct. Biol. 21 (2011) 802–807.
[8] X. Prasanna, M. Mohole, A. Chattopadhyay, D. Sengupta, Chem. Phys. Lipids 227 (2020) 104852.
[9] A.J.Y. Jones, F. Gabriel, A. Tandale, D. Nietlispach, Molecules 25 (2020) 1–39.
[10] R. Baccouch, E. Rascol, K. Stoklosa, I.D. Alves, Biophys. Chem. 285 (2022) 106794.
[11] R. Dawaliby, C. Trubbia, C. Delporte, M. Masureel, P. Van Antwerpen, B. K. Kobilka, C. Govaerts, Nat. Chem. Biol. 12 (2016) 35–39.
[12] M.J. Strohman, S. Maeda, D. Hilger, M. Masureel, Y. Du, B.K. Kobilka, Nat. Commun. 10 (2019) 1–10.
[13] K.E. Komolov, Y. Du, N.M. Duc, R.M. Betz, J.P.G.L.M. Rodrigues, R.D. Leib, D. Patra, G. Skiniotis, C.M. Adams, R.O. Dror, K.Y. Chung, B.K. Kobilka, J. L. Benovic, Cell 169 (2017) 407–421.e16.
[14] D.P. Staus, H. Hu, M.J. Robertson, A.L.W. Kleinhenz, L.M. Wingler, W.D. Capel, N. R. Latorraca, R.J. Lefkowitz, G. Skiniotis, Nature 579 (2020) 297–302.
[15] Y.H.M. Chan, S.G. Boxer, Curr. Opin. Chem. Biol. 11 (2007) 581–587.
[16] A. Chen, E.J. Majdinasab, M.C. Fiori, H. Liang, G.A. Altenberg, Front. Bioeng. Biotechnol. 8 (2020) 598450.
[17] M. Orwick-Rydmark, J.E. Lovett, A. Graziadei, L. Lindholm, M.R. Hicks, A. Watts, Nano Lett. 12 (2012) 4687–4692.
[18] S. Gulati, M. Jamshad, T.J. Knowles, K.A. Morrison, R. Downing, N. Cant, R. Collins, J.B. Koenderink, R.C. Ford, M. Overduin, I.D. Kerr, T.R. Dafforn, A. J. Rothnie, Biochem. J 461 (2014) 269–278.
[19] M. Jamshad, J. Charlton, Y.P. Lin, S.J. Routledge, Z. Bawa, T.J. Knowles, M. Overduin, N. Dekker, T.R. Dafforn, R.M. Bill, D.R. Poyner, M. Wheatley, Biosci. Rep. 35 (2015) 1–10.
[20] D.J.K. Swainsbury, S. Scheidelaar, N. Foster, R. van Grondelle, J.A. Killian, M. R. Jones, Biochim. Biophys. Acta—Biomembr. (1859, 2017,) 2133–2143.
[21] S. Rehan, V.O. Paavilainen, V.P. Jaakola, Biochim. Biophys. Acta—Biomembr. 2017 (1859) 1059–1065.
[22] Y. Liu, E.C.C.M. Moura, J.M. Dörr, S. Scheidelaar, M. Heger, M.R. Egmond, J. A. Killian, T. Mohammadi, E. Breukink, PLoS One 13 (2018) 1–18.
[23] S. Scheidelaar, M.C. Koorengevel, C.A. van Walree, J.J. Dominguez, J.M. Dörr, J. A. Killian, Biophys. J. 111 (2016) 1974–1986.
[24] A.H. Kopf, J.M. Dörr, M.C. Koorengevel, F. Antoniciello, H. Jahn, J.A. Killian, Biochim. Biophys. Acta—Biomembr. 1862 (2020) 183125.

[25] M.C. Fiori, Y. Jiang, G.A. Altenberg, H. Liang, Sci. Rep. 7 (2017) 1–10.
[26] M.C. Fiori, W. Zheng, E. Kamilar, G. Simiyu, G.A. Altenberg, H. Liang, Sci. Rep. 10 (2020) 1–13.
[27] A.O. Oluwole, B. Danielczak, A. Meister, J.O. Babalola, C. Vargas, S. Keller, Angew. Chem. Int. Ed. 56 (2017) 1919–1924.
[28] A.O. Oluwole, J. Klingler, B. Danielczak, J.O. Babalola, C. Vargas, G. Pabst, S. Keller, Langmuir 33 (2017) 14378–14388.
[29] M. Barniol-Xicota, S.H.L. Verhelst, J. Am. Chem. Soc. 140 (2018) 14557–14561.
[30] A.A. Gulamhussein, R. Uddin, B.J. Tighe, D.R. Poyner, A.J. Rothnie, Biochim. Biophys. Acta—Biomembr. 1862 (2020) 183281.
[31] V.J. Flegler, A. Rasmussen, S. Rao, N. Wu, R. Zenobi, M.S.P. Sansom, R. Hedrich, T. Rasmussen, B. Böttcher, Proc. Natl. Acad. Sci. 117 (2020) 28754–28762.
[32] B. Danielczak, M. Rasche, J. Lenz, E.P. Patallo, S. Weyrauch, F. Mahler, M. T. Agbadaola, A. Meister, J.O. Babalola, C. Vargas, C. Kolar, S. Keller, Nanoscale 14 (2022) 1855–1867.
[33] J. Lenz, A.H. Larsen, S. Keller, A. Luchini, Langmuir 39 (2023) 3569–3579.
[34] A. Mattarei, M. Azzolini, M. Zoratti, L. Biasutto, C. Paradisi, Molecules 20 (2015) 16085–16102.
[35] D. Lin-Vien, N.B. Colthup, W.G. Fateley, J.G. Grasselli, The Handbook of Infrared and Raman Characteristic Frequencies of Organic Molecules, Elsevier, 1991.
[36] G. Socrates, G. Socrates, Infrared and Raman Characteristic Group Frequencies: Tables and Charts, third ed., Wiley, Chichester; New York, 2001.
[37] P. Gill, T.T. Moghadam, B. Ranjbar, J. Biomol. Technol. 21 (2010) 167–193.
[38] J.C.W. Corbett, M.T. Connah, K. Mattison, Electrophoresis 32 (2011) 1787–1794.
[39] T.W. Herling, D.J. O'Connell, M.C. Bauer, J. Persson, U. Weininger, T.P.J. Knowles, S. Linse, Biophys. J. 110 (2016) 1957–1966.
[40] D.E. Otzen, A.K. Buell, H. Jensen, Curr. Opin. Struct. Biol. 70 (2021) 8–15.
[41] J.A. Ballesteros, H. Weinstein, in: Methods in Neurosciences, Academic Press, 1995, pp. 366–428.
[42] J. Yu, L.E. Gimenez, C.C. Hernandez, Y. Wu, A.H. Wein, G.W. Han, K. McClary, S. R. Mittal, K. Burdsall, B. Stauch, L. Wu, S.N. Stevens, A. Peisley, S.Y. Williams, V. Chen, G.L. Millhauser, S. Zhao, R.D. Cone, R.C. Stevens, Science 368 (2020) 428–433.
[43] K. Janson, J. Zierath, F.L. Kyrilis, D.A. Semchonok, F. Hamdi, I. Skalidis, A.H. Kopf, M. Das, C. Kolar, M. Rasche, C. Vargas, S. Keller, P.L. Kastritis, A. Meister, Biochim. Biophys. Acta—Biomembr. 1863 (2021) 183725.
[44] D. Glueck, A. Grethen, M. Das, O.P. Mmeka, E.P. Patallo, A. Meister, R. Rajender, S. Kins, M. Räschle, J. Victor, C. Chu, M. Etzkorn, Z. Köck, F. Bernhard, J. O. Babalola, C. Vargas, S. Keller, Small 18 (2022) 2202492.
[45] M.J. Agulleiro, R. Cortés, B. Fernández-Durán, S. Navarro, R. Guillot, E. Meimaridou, A.J.L. Clark, J.M. Cerdá-Reverter, Mol. Endocrinol. 27 (2013) 1934–1945.
[46] M. Jamshad, V. Grimard, I. Idini, T.J. Knowles, M.R. Dowle, N. Schofield, P. Sridhar, Y. Lin, R. Finka, M. Wheatley, O.R.T. Thomas, R.E. Palmer, M. Overduin, C. Govaerts, J.M. Ruysschaert, K.J. Edler, T.R. Dafforn, Nano Res. 8 (2015) 774–789.
[47] V. Postis, S. Rawson, J.K. Mitchell, S.C. Lee, R.A. Parslow, T.R. Dafforn, S. A. Baldwin, S.P. Muench, Biochim. Biophys. Acta—Biomembr. (1848, 2015,) 496–501.
[48] J. Broecker, B.T. Eger, O.P. Ernst, Structure 25 (2017) 384–392.
[49] S.C. Lee, R. Collins, Y.P. Lin, M. Jamshad, C. Broughton, S.A. Harris, B.S. Hanson, C. Tognoloni, R.A. Parslow, A.E. Terry, A. Rodger, C.J. Smith, K.J. Edler, R. Ford, D.I. Roper, T.R. Dafforn, Sci. Rep. 9 (2019) 1–16.
[50] S. Lindhoud, V. Carvalho, J.W. Pronk, M.E. Aubin-Tam, Biomacromolecules 17 (2016) 1516–1522.
[51] T. Ravula, N.Z. Hardin, S.K. Ramadugu, A. Ramamoorthy, Langmuir 33 (2017) 10655–10662.
[52] M. Esmaili, B.P. Tancowny, X. Wang, A. Moses, L.M. Cortez, V.L. Sim, H. Wille, M. Overduin, J. Biol. Chem. 295 (2020) 8460–8469.
[53] M. Esmaili, C. Acevedo-Morantes, H. Wille, M. Overduin, Biochim. Biophys. Acta—Biomembr. 1862 (2020) 183360.
[54] S.C.L. Hall, C. Tognoloni, J. Charlton, E.C. Bragginton, A.J. Rothnie, P. Sridhar, M. Wheatley, T.J. Knowles, T. Arnold, K.J. Edler, T.R. Dafforn, Nanoscale 10 (2018) 10609–10619.
[55] O.P. Hawkins, C.P.T. Jahromi, A.A. Gulamhussein, S. Nestorow, T. Bahra, C. Shelton, Q.K. Owusu-Mensah, N. Mohiddin, H. O'Rourke, M. Ajmal, K. Byrnes, M. Khan, N.N. Nahar, A. Lim, C. Harris, H. Healy, S.W. Hasan, A. Ahmed, L. Evans, A. Vaitsopoulou, A. Akram, C. Williams, J. Binding, R.K. Thandi, A. Joby, A. Guest, M.Z. Tariq, F. Rasool, L. Cavanagh, S. Kang, B. Asparuhov, A. Jestin, T.R. Dafforn, J. Simms, R.M. Bill, A.D. Goddard, A.J. Rothnie, Biochim. Biophys. Acta—Biomembr. 1863 (2021) 183758.